Bioluminescence resonance energy transfer–based imaging of protein–protein interactions in living cells

Hiroyuki Kobayashi, Louis-Philippe Picard, Anne-Marie Schönegge and Michel Bouvier [ORCID]*

Bioluminescence resonance energy transfer (BRET) is a transfer of energy between a luminescence donor and a fluorescence acceptor. Because BRET occurs when the distance between the donor and acceptor is <10 nm, and its efficiency is inversely proportional to the sixth power of distance, it has gained popularity as a proximity-based assay to monitor protein–protein interactions and conformational rearrangements in live cells. In such assays, one protein of interest is fused to a bioluminescent energy donor (luciferases from *Renilla reniformis* or *Oplophorus gracilirostris*), and the other protein is fused to a fluorescent energy acceptor (such as GFP or YFP). Because the BRET donor does not require an external light source, it does not lead to phototoxicity or autofluorescence. It therefore represents an interesting alternative to fluorescence-based imaging such as FRET. However, the low signal output of BRET energy donors has limited the spatiotemporal resolution of BRET imaging. Here, we describe how recent improvements in detection devices and BRET probes can be used to markedly improve the resolution of BRET imaging, thus widening the field of BRET imaging applications. The protocol described herein involves three main stages. First, cell preparation and transfection require 3 d, including cell culture time. Second, image acquisition takes 10–120 min per sample, after an initial 60 min for microscope setup. Finally, image analysis typically takes 1–2 h. The choices of energy donor, acceptor, luminescent substrates, cameras and microscope setup, as well as acquisition modes to be used for different applications, are also discussed.

Introduction

Protein trafficking and interactions with different partners are at the core of most physiological responses. Monitoring these processes in real time in living cells provides important information about the spatiotemporal regulation of multiple cell functions. In recent years, the use of fluorescence and luminescence tools has led to major breakthroughs in our understanding of cellular dynamics, by allowing monitoring of movement and interaction of proteins. Among the approaches used, RET has gained in popularity.

RET is a natural phenomenon occurring between two photoactive molecules[1]. It corresponds to the transfer of energy from a donor to an acceptor molecule through a non-radiative resonance process occurring through dipole–dipole coupling that happens only at a permissive distance and proper orientation. The transfer of energy results in the excitation of the acceptor, which then emits light at a specific wavelength. Two types of RET phenomenon have been mainly used to monitor biological processes: fluorescence RET (FRET)[2,3] and BRET[4,5], which use fluorescent and luminescent donors, respectively. For most RET pairs, efficient transfer can occur only if the distance between the donor and the acceptor is <10 nm, and the efficiency of transfer decreases as a function of the sixth power of the distance between them. The average size of a protein being $\cong$5 nm, changes in RET between donors and acceptors fused to proteins of interest reflect changes in the distance between the tagged proteins, which are consistent with the occurrence of macromolecular rearrangements. As a result, RET assays have been widely used to characterize protein–protein interactions and conformational changes within proteins or protein complexes.

BRET has been extensively used to investigate G protein–coupled receptor (GPCR) dynamics and signaling activity. For instance, BRET-based assays have been used to study receptor multi-merization[4,6,7], coupling to and activation of G protein[8,9], trafficking[10], engagement and activation of accessory proteins, such as β-arrestins[11–15] and receptor activity–modifying proteins[16], as well as

Institute for Research in Immunology and Cancer (IRIC), Université de Montréal, Montreal, QC, Canada. *e-mail: michel.bouvier@umontreal.ca
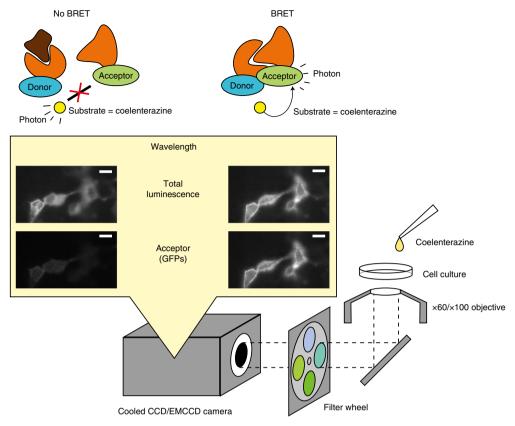
Fig. 1 | Overview of the setup for BRET microscopy. Microscope elements needed for image acquisition. From right to left: substrate and cells to generate the light, objective with magnification, filter wheel to select the wavelength needed and the high-sensitivity/low-background camera to capture the image. In the example pictures, HEK293 cells were transfected with V2 vasopressin receptor, β-arrestin2-RlucII and rGFP-CAAX. Images were obtained before (no BRET) or 10 min after (BRET) the addition of vasopressin receptor ligand (100 nM arginine vasopressin) without a filter (total luminescence) or with an acceptor 480-nm longpass filter (480LP). The substrate was 10 µM Me-O-e-CTZ. Scale bars, 20 µm.

post-translational modifications, such as ubiquitination[17]. More recently, BRET has also been used for ligand-binding assays using fluorophore-conjugated ligands and a receptor fused to an energy donor[18,19]. In most cases, the BRET signal was quantified by spectrometric measures using luminometers equipped with a monochromator or filters separating the donor and acceptor emissions. Classically, BRET is quantified by dividing the light signal of the acceptor by the luminescence emitted by the donor. Although useful, such spectrometric studies cannot provide information about the subcellular localization of the processes monitored. Although it has been difficult to image BRET signals with high spatial resolution because of the low light output of luciferase (the energy-luminescent donor), recent enzymatic improvement[20] of *Renilla* luciferase (Rluc)-based BRET donors and the development of new luciferases such as NanoLuc (Nluc)[21] have improved signal strength markedly, allowing the development of BRET imaging approaches, including imaging of protein–protein interactions in culture cells[22–27] and even in living animals, using red-shifted BRET probes[28,29] that overcome tissue absorption. In this protocol, we present procedures for BRET-based microscopic visualization of protein–protein interactions and trafficking that combine recent improvements in ultra-low-light detectors, new generations of BRET probes and new approaches, such as enhanced bystander BRET (ebBRET)[26,27]. GPCR activation and trafficking are used as an example of the biological systems that can be studied using such high-resolution BRET microscopy imaging.

The protocol provides all the information needed to select the best BRET pairs and detection systems for different applications, as well as presenting the advantages and disadvantages of the different approaches. In addition, the step-by-step procedure allows investigators to easily perform BRET imaging experiments.

The major components of the BRET imaging microscopy system are illustrated in Fig. 1. The system used in the present protocol is composed of an inverted microscope connected to an

electron-multiplying CCD (EMCCD) camera through a regular port equipped with a motorized filter wheel. The motorized system allows rapid switching between filter-on (GFP emission) or filter-off (corresponding to the entire light emitted, which is used as a measure of the donor emission). Because BRET is a luminescence-based assay, it does not require external illumination, but a light source for bright-field or epi-fluorescence microscopy is required for focusing purposes. Luminescence is produced by the direct application of the luciferase substrate to the cells.

Comparison with other methods

Unlike most other protein–protein interaction assays, such as co-immunoprecipitation, pull-down, protein ligation assays[30] or cross-linking assays, RET-based assays can directly monitor protein–protein interactions in living cells. This noninvasive characteristic of the RET assay is particularly useful when the properties of the interacting proteins can be changed by their extraction or purification, or when the influence of the cellular environment is being studied. Another assay that allows the detection of protein–protein interaction in living cells is the protein complementation assay (PCA)[31]. PCA imaging is based on the reconstitution of a reporter protein (typically fluorescent proteins or luminescent enzymes) from its split fragments fused to the proteins of interest. Therefore, the PCA signal can be detected only when two PCA fragments reconstitute the functional reporter as a consequence of the interaction of the fusion proteins. Although this assay can provide robust signals, the background signal can be relatively high because of the propensity of some of the fragments to self-associate. In addition, the dynamics of the interactions can also be affected by the complementation process itself, because reconstitution of the reporter protein can stabilize the complex. Unlike RET assays, which allow the quantitative monitoring of each of the partners (by monitoring luminescence and fluorescence independently), with PCA no information can be directly obtained about the quantity or distribution of the noninteracting fragments. Despite these limitations, PCA remains a useful type of assay. In particular, modifications of the interacting fragments to reduce their affinity for one another have been used to considerably reduce the possible artifact linked to the self-association of the fragments[32]. Also, PCA using split firefly luciferase[33], Rluc[34], Nluc (NanoBit)[35] or split fluorescent proteins[36] has been combined with BRET to monitor the formation of up to four multiprotein complexes[37–39].

Many RET-based microscopic imaging methods have been developed to monitor biological processes in the specific subcellular compartments where they occur. One of the major challenges of RET imaging is that of separating weak energy transfer signals from background. For that reason, FRET has been favored over BRET for imaging purposes because the level of signal resulting from the excitation (by light) of a fluorescent donor is greater than that from the bioluminescent donors used for BRET. However, the strong external illumination in FRET assays also increases the background autofluorescence signal, which can limit the signal resolution of FRET imaging. Off-peak excitation of the acceptor by the donor excitation light source is also a source of contamination that is dependent on the amount of acceptor, which is why acceptor photobleaching or fluorescence lifetime–FRET imaging is often used. The strong FRET illumination also causes phototoxicity and photobleaching, making long time-lapse measurement difficult. By contrast, BRET does not require an external light-mediated excitation of the donor because the energy emitted results from a bioluminescent reaction involving the oxidation of a substrate. It follows that no autofluorescence occurs, yielding a good signal-to-noise ratio (SNR). However, the low-light intensity characteristic of BRET assays requires a much more sensitive system for signal detection (see the 'Limitations' section below).

Limitations

Most of the BRET imaging limitations are related to the ability to collect sufficient light to obtain high-resolution images. This limitation depends on the brightness of the partners, the energy transfer efficiency of the sensor pair used and the kinetics of the phenomenon studied. It follows that BRET probes expressed at low levels are more difficult to image. Longer acquisition times can be used to mitigate this limitation to some extent. However, longer acquisition times limit the ability to image real-time dynamics because (i) the time required to generate a sufficiently high-quality image may be longer than the timescale of the phenomenon that is being investigated or (ii) the time required is longer than the lifetime of the luminescent signal. The low intensity of light may also make it more difficult to obtain valid quantification of the BRET changes observed. This is partly true when the signal of interest is close to the shot noise (the statistical random fluctuation of the photon counts).

To mitigate these limitations, selection of the brightest BRET partners and substrates, as well as the use of efficient optics and sensitive detectors is of primary importance. In the examples shown in this protocol, the minimum acquisition time to obtain images for both total luminescence and energy acceptor channels is 25 s. It follows that real-time kinetic analyses are limited to phenomena occurring on a timescale >25 s. Although this allows the quantitative assessment of phenomena such as receptor endocytosis[40] or β-arrestin recruitment[41], it does not permit the real-time analysis of G-protein activation[42], for example.

One of the advantages of BRET imaging over spectrometric (plate reader) BRET measurement is the possibility of assessing the subcellular origin of the signal. However, the subcellular resolution remains moderate and does not allow easy distinction of discrete subcellular organelles. One of the problems leading to lack of resolution is the extent of time needed to detect sufficient signal. Indeed, cellular movements occurring during the acquisition period will lead to blurred images and could even have an impact on the accuracy of the BRET values calculated for a specific pixel. To limit this effect, we recommend never exceeding an acquisition time of 10 s (100 × 100-ms frames) for each wavelength + 5 s for processing, so that the measurements of the two wavelengths are performed within a time interval during which relatively small changes of shape or cell movement occur. For measurements that require longer acquisition times because of the low intensity of the signals, we recommend performing several rounds (up to ten) of 25-s measurements (10 s for each wavelength + 5 s for processing), and the integration of each of the images that are not substantially affected by cell movement or cell-shape changes. This allows increased accuracy of BRET measurements at a specific location.

Experimental design

Energy donors and acceptors

The most frequently used BRET donor is Rluc, an oxidase isolated from the bioluminescent sea pansy, *R. reniformis*. In the original BRET assays, the native Rluc was used[4,5]. However, Rluc mutants, such as Rluc8 (A55T, C124A, S130A, K136R, A143M, M185V, M253L and S287L)[20] or RlucII (A55T, C124A and M185V)[43,44] have improved enzymatic activity, providing greater brightness and making them donors of choice for BRET imaging. More recently, another luciferase from the sea shrimp, *O. gracilirostris*, known as Nluc[21], has also emerged as a good choice for some BRET applications (see 'Additional BRET donors' section below).

The fluorophores used as BRET acceptors usually belong to the family of GFPs, originating either from *Aequorea victoria* or *R. reniformis*. The best fluorophores are selected on the basis of their excitation and emission spectra (depending on the donor/substrate used), as well as their quantum yield and Stokes' shift[45]. The BRET signal can have different characteristics depending on the nature of the luciferases used as donors, the luciferase substrates and the acceptor selected. Different combinations and their advantages and limitations are described in the following sections.

BRET1 assays

Rluc catalyzes the oxidation of its native substrate, coelenterazine (CTZ), into coelenteramide, and the relaxation of coelenteramide to the ground state produces luminescence with an emission peak at ~480 nm[46]. GFP variants having an excitation wavelength that overlaps this emission spectrum, such as eYFP (excitation: 514 nm) or Venus-GFP (excitation: 515 nm)[47], can be used as BRET acceptors for the Rluc-CTZ donor couple and are used in so-called BRET1 assays. A synthetic CTZ analog, CTZh (2-deoxy CTZ), is also often used as a substrate for BRET1 assays, showing results similar to those obtained with CTZ.

BRET1 was the first BRET assay format developed for protein–protein interaction analyses[4,5]. Because the wavelength profile of BRET1 is similar to that of the frequently used CFP and YFP FRET pairs, devices and constructs already available made it easy to perform BRET1 experiments. However, a major drawback of BRET1 is the poor signal separation between the donor and acceptor emission wavelengths, resulting in a suboptimal SNR. As shown in Fig. 2a, the donor and acceptor emission spectra for BRET1 pairs have a large overlap because the spectral width of Rluc-CTZh luminescence (≈85 nm) is much larger than the Stokes' shift of eYFP (≈15 nm). It follows that the acceptor signal is not well resolved from the contaminating donor signal, making it difficult to quantify, especially when the efficiency of transfer is low.
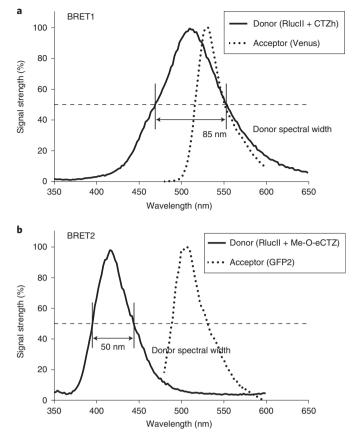
Fig. 2 | Comparison of spectral characteristics of BRET assay constructs. a, The emission spectrum of the donor luminescence and acceptor fluorescence for BRET1. The solid curve shows BRET1 donor (RlucII + CTZh) luminescence reaching a maximum at 512 nm (bandwidth of 85 nm), and the dashed curve shows the BRET1 acceptor (Venus) fluorescence reaching a maximum at 532 nm (20 nm longer than the donor maximum). **b**, The emission spectrum of donor luminescence and acceptor fluorescence for BRET2. The solid curve shows the BRET2 donor (RlucII + Me-O-e-CTZ) luminescence reaching a maximum at 417 nm (bandwidth of 50 nm), and the dashed curve shows the BRET2 acceptor (GFP2) fluorescence reaching a maximum at 506 nm (89 nm longer than the donor maximum). All spectrum measurements were performed in a white 96-well plate containing HEK293 cells transiently expressing RlucII, along with either Venus or GFP2 for BRET1 or BRET2, respectively, using a microplate luminescence/fluorescence reader (Synergy Neo2).

BRET2 assays

BRET2 was developed with the objective of increasing the separation between the donor and acceptor emission spectra, so as to improve signal-to-background ratio[14]. BRET2 uses synthetic CTZ analogs, such as CTZ400A (also known as DeepBlueC or bisdeoxy-CTZ) or Me-O-e-CTZ (also known as Prolume Purple), which emits blue-shifted luminescence peaking at ~400 nm when oxidized by Rluc[20]. The emission of these substrates has a narrower spectral width than the substrates used for BRET1 (~50 versus 85 nm, Fig. 2b). BRET2 acceptors include *A. victoria* GFP mutants, such as GFP10 (ref. [48]) or GFP2 (ref. [14]), which have much larger Stokes' shift than YFP (~90 versus 15 nm) and can be efficiently excited with blue-shifted luminescence. As a result, BRET2 provides greater signal separation than BRET1, resulting in a greater dynamic window (see Anticipated results). However, the luminescence signal of BRET2 tends to be weaker than that of BRET1, due to the low light output of blue-shifted substrates, and may be more difficult to monitor depending on the detection systems used. Figure 3 illustrates the difference in luminescence emitted by the substrates used for BRET1 and BRET2. The BRET1 substrate, CTZh, generates luminescence signals that are 3–17 times brighter than the three blue-shifted CTZ analogs tested (Fig. 3a). Among the blue-shifted substrates, Me-O-e-CTZ and Me-O-CTZ-O-Me (also known as Prolume Purple II) are brighter than CTZ400A, which was the original substrate described for BRET2 (ref. [14]). Another limitation of BRET2 is that all blue-shifted substrates show a much faster signal decay (half-life ≈12 min) as compared to CTZh (half-life ≈22 min) (Fig. 3b). This difference in the half-life of luminescence can be easily appreciated in luminescence images taken from cells expressing RlucII-tagged β-arrestin2.
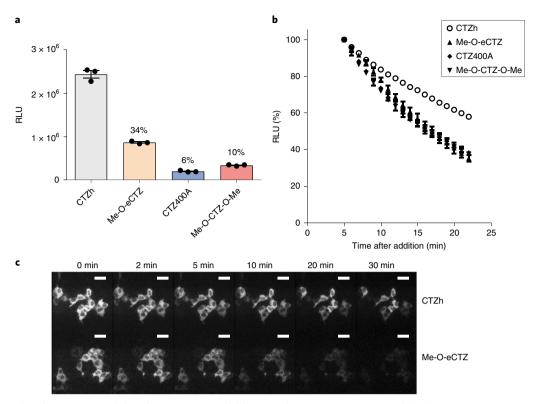
Fig. 3 | Comparison of RlucII luminescence with different substrates. a, Comparison of the luminescence intensity 5 min after the addition of substrates. The values on the top of each bars represent the mean ± s.e.m. ($n = 3$) of the percentage of the CTZh signal intensity. **b**, Time-dependent decay of luminescence signal for different substrates. Data are the mean ± s.e.m. of three independent experiments. In **a** and **b**, luminescence measurements were performed using the Synergy Neo2 microplate reader on HEK293 cells transiently expressing RlucII and re-suspended in a 96-well plate with a 1 μM final concentration of substrates. **c**, Comparison of the signal decay of CTZh and Me-O-e-CTZ in luminescence imaging. HEK293 cells were transfected with β-arrestin2-RlucII, and the total luminescence image was continuously obtained with an exposure time of 10 s. Images at 0, 2, 5, 10, 20 and 30 min are shown. The substrates were added at a 10 μM final concentration. The grayscale levels of the photos correspond to 0–30 photons (CTZh), and 0–10 photons (Me-O-e-CTZ). Scale bars, 40 μm. RLU, relative luminescence units from microplate reader.

Indeed, the luminescence following CTZh addition is easily detectable for >30 min, whereas the image obtained with Me-O-e-CTZ as the substrate decayed rapidly and was barely detectable after 10 min (Fig. 3c).

Additional BRET acceptors

The GFP from *R. reniformis* (rGFP), can be used as a BRET acceptor that also allows a good separation between donor and acceptor emissions (Fig. 4). It also results in a larger BRET signal due to a better transfer efficiency between Rluc and rGFP[49] than between Rluc and GFPs from other species. Indeed, the fact that the two proteins co-evolved in the same species resulted in an optimal dipole orientation for transfer in the Rluc-rGFP dimer[50]. The very efficient transfer can easily be seen when comparing BRET images obtained for the Rluc-rGFP to Rluc-GFP10 fusion constructs (Fig. 4a, two last rows). However, the fact that rGFP spontaneously interacts with Rluc precludes the use of this energy acceptor for studying protein–protein interactions. Yet this propensity of the Rluc and rGFP pair to interact with one another (albeit with low affinity) can be used to increase the signal originating from random collisions known as bystander BRET. This property has recently been used to monitor the localization of protein in specific subcellular domains[26]. For instance, such ebBRET can readily detect the translocation of Rluc-fused proteins to a specific subcellular domain or organelle harboring rGFP targeted to these sites with specific subcellular localization motifs. In such cases, Rluc spontaneously interacts with rGFP, enabling efficient BRET energy transfer only if Rluc and rGFP are in the same subcellular compartment (see 'Anticipated results').
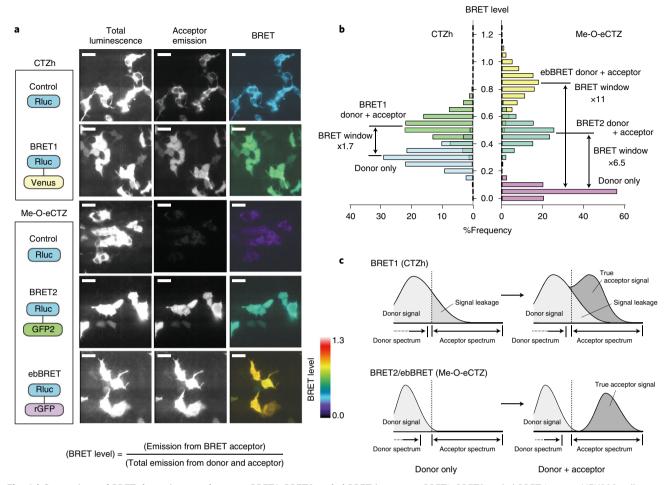
Fig. 4 | Comparison of BRET dynamic range between BRET1, BRET2 and ebBRET images. a, BRET1, BRET2 and ebBRET images: HEK293 cells were transfected with fusion proteins encoding Venus-RlucII for BRET1, GFP2-RlucII for BRET2, rGFP-RlucII for ebBRET and β-arrestin2-RlucII as a control. In the FP-RlucII fusion proteins, a linker of 19 amino acids was used to connect GFP2, YFP or rGFP to RlucII. In each image, BRET levels (the ratio of the acceptor photon count to the total photon count) are expressed as a heat map color code (lowest being black and purple, and highest being red and white), as shown in the bottom-right corner of the panel. Scale bars, 20 μm. **b**, Comparison of BRET levels between images from **a**: BRET levels are calculated as the ratio between the luminescence from the BRET acceptor and the total luminescence signal from all pixels showing >50 photon counts. The distribution of BRET levels is expressed as a histogram. The bin width of the histogram is 0.05 arbitrary BRET values and is plotted against relative frequency for each bin. The values in the figure represent dynamic BRET windows (BRET from donor + acceptor constructs/BRET from donor construct only) calculated using the mean values of each of the distributions. **c**, Emission spectra for donor alone versus donor + acceptor conditions: photon counts correspond to the donor emission leaking into the acceptor spectrum and the true donor emission for BRET1, BRET2 and ebBRET. The equation used to calculate BRET levels is described at the bottom of **a**.

Additional BRET donors

In addition to *Renilla* luciferase, luciferases from different animal species, firefly *Photinus pyralis*[51], copepod *Gaussia princeps*[52] and deep-sea shrimp *O. gracilirostris*[18], have also been used in BRET applications. As reported by several groups[24,25], the *Oplophorus* luciferase is especially interesting for BRET imaging because engineered luciferases based on the *Oplophorus* enzyme, such as eKAZ[53] and Nluc[21] show greater light output than Rluc, and their catalytic subunits (19 kDa) are smaller than that of Rluc (34 kDa)[54]. The enzymatic activity of Nluc[21], similar to that of Rluc[55,56], is more stable than firefly luciferase under different environmental conditions such as temperature, pH and salt concentration. These advantageous characteristics of Nluc led to the development of novel Nluc-based applications, such as ligand-binding assays using Nluc complementation[57] and BRET with fluorophore-conjugated ligands[58]. Although *Oplophorus* luciferases can use CTZ analogs as substrates[46,53], it should be noted that the emission wavelength and light intensity obtained for various analogs are different from those obtained with Rluc (Fig. 5). For instance, Rluc substrates such as Me-O-e-CTZ and Me-O-CTZ-O-Me do not show luminescence with Nluc, whereas another Rluc substrate, CTZ400A, as well as the Nluc substrate furimazine, generated brighter signals with 5.2 and 3.4 times greater light output than CTZh when used with Nluc (Fig. 5a). Interestingly, CTZ400A, which
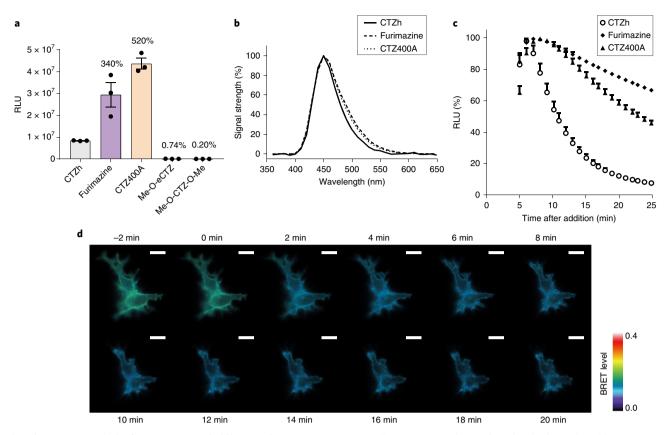
Fig. 5 | Comparison of Nluc luminescence with different substrates. a–c, HEK293 cells were transiently transfected with Nluc and total luminescence was measured after the addition of 1 μM substrate (final concentration) using a Synergy Neo2. **a** Comparison of the luminescence intensity 5 min after addition of substrates to the cells. The values on the top of each bar represent the mean ± s.e.m. ($n = 3$) of the percentage of the CTZh signal intensity. **b**, Luminescence spectra of different Nluc substrates. **c**, Time-dependent decay of luminescence signal of different substrates; the data represent the mean ± s.e.m. ($n = 3$). **d**, BRET imaging of the interaction between Gαq-Nluc, Gβ1 and CyOFP-Gγ1. HEK293 cells were transiently transfected with Gαq-Nluc (Nluc is inserted at position 118 of Gαq), Gβ1 and CyOFP-Gγ1, and BRET images were obtained after the addition of 10 μM CTZ400A and treatment with 100 nM angiotensin II (AT1R agonist) for 20 min. The BRET levels are expressed using a heat map as described in Fig. 4a. The pixel brightness represents the total photon count of each pixel. Scale bars, 10 μm.

emits light at 400 nm with Rluc (blue-shifted compared to CTZh), does not show such a blue-shifted spectrum with Nluc, and the peak emission is observed at 460 nm, similar to what is observed with other CTZ analogs, such as CTZh and furimazine (Fig. 5b). This means that CTZ400A represents the brightest and cheapest alternative for Nluc-based assays. However, the luminescence decay for furimazine is slower than that of CTZ400A when using Nluc, a property that could make it a better alternative for long real-time imaging. An advantage of Nluc for BRET imaging is the much slower decay of the luminescent signal, as compared to that of Rluc, for all substrates tested (compare Figs. 3b and 5c), allowing the possibility of longer acquisition times to monitor the kinetics of biological processes (Fig. 5d). This characteristic has been taken advantage of in recent studies monitoring ligand-binding kinetics using BRET-based assays with Nluc[57,58], as well as for real-time BRET imaging of processes occurring over a timescale going from minutes to an hour[25]. However, Nluc cannot be used for ebBRET experiments, and thus Rluc still represents an advantageous alternative energy donor that is useful for some applications. It should also be noted that many biosensors using Rluc have already been developed and validated and can be readily used for BRET imaging. Novel Nluc-based sensors will certainly be developed but will require rigorous validation before they become available for imaging.

How to select a BRET donor and acceptor
The choice of the donor–acceptor pairs to use for BRET imaging largely depends on the specific process being imaged. Whether or not real-time imaging is sought, the timescale of imaging needed and the availability of already-validated biosensors are parameters that will influence the choice of BRET pairs.

For many applications, Rluc can be used as the donor in BRET1 (substrate: CTZh; acceptor: Venus) or BRET2 (substrate: CTZ400A or Me-O-e-CTZ; acceptor: GFP10 or GFP2) configurations. If the expression level of the protein fused to the energy donor is low, BRET1 using Venus as the acceptor would be preferable to GFP10 or GFP2 because it provides higher light output. However, if sufficient luminescence can be detected using blue-shifted substrates for Rluc (CTZ400A or Me-O-e-CTZ), GFP2 or GFP10 could be better acceptor choices because BRET2 provides a greater dynamic window. In the case in which the luminescence signal generated by Rluc with any substrate is too low, Nluc is the preferred choice when using either *A. victoria* YFP variants[25] or the newly characterized *Discosoma* coral variants, cyan-excitable orange fluorescent protein (CyOFP) and cyan-excitable RFP (CyRFP) with furimazine or CTZ400A as substrates. These fluorescent protein variants have excitation peaks similar to that of Venus (≈500 nm) but have a larger Stokes' shift than Venus, yielding a greater separation between donor and acceptor emissions, thus opening possibilities of developing new generations of BRET imaging sensors[59,60]. Figure 5d illustrates the use of Nluc to image the dissociation of Gαq-Nluc from CyOFP-Gγ1 upon sustained stimulation with the angiotensin-II type-1 receptor (AT1R) agonist angiotensin II for 20 min. BRET-based ligand-binding assays using Nluc and the red-shifted fluorophore BODIPY 630/650 also took advantage of such larger Stokes' shifts[18]. Although Nluc can clearly be advantageous for many applications, the existence of many validated sensors based on Rluc also makes that energy donor an appealing choice in many cases, as long as the expression levels are sufficient.

For real-time imaging applications, although Rluc-based BRET1, BRET 2 or Nluc-based BRET can all be used, the timescale of the process to image will determine the best choice. The imaging time being limited by the intensity and the half-life of the luminescence emission, Nluc-based BRET using either furimazine or CTZ400A would be the preferred energy donor because of its brightness and the long emission half-life (≈30 min), allowing imaging for a few hours. The next best choice would be BRET1, which provides ≈10 times less light than Nluc but three times more light than BRET2, with a half-life of ≈22 min, limiting the imaging to ≈1 h. Finally, BRET2 can also be used, but the lower light output and the shorter half-life of the signal (≈12 min) greatly limit the imaging time, which cannot extend to >≈20 min.

Although fluorescent proteins have been used more frequently as BRET energy acceptors, chemical fluorophores can also be used successfully for imaging[19,61]. Generally speaking, the spectrometric properties of chemical fluorophores are superior to those of fluorescent proteins, and good acceptors can be found for all BRET donors. However, the methods of conjugating the fluorophore to the protein of choice must be developed and optimized for each sensor.

To monitor protein translocation, ebBRET using Rluc as the donor, rGFP as the acceptor and Me-O-e-CTZ as the substrate, is the superior choice. Both the excellent SNR and greater efficiency of transfer (due to the direct association of Rluc and rGFP, Fig. 4a) allow very robust monitoring of protein trafficking (see 'Anticipated results') that cannot be readily imaged using BRET1, BRET2 or Nluc-based BRET.

Distinguishing signal from noise

The above sections describe a number of novel donor–acceptor pairs with improved properties that allow their use for spatiotemporally resolved BRET imaging in various conditions. Still, one of the main limitations of BRET imaging remains the low level of the light output, which makes it difficult to distinguish it from noise. The main source of the noise for such low-level signals originates from the statistically random fluctuation of the photon counts that is known as 'shot noise'. When considering only the shot noise, the SNR increases as the square root of the incoming photon number. It follows that to increase the SNR of BRET images by twofold, the amount of light emitted must be increased by fourfold. Accordingly, the BRET imaging experiment should be designed to maximize the signal output while constraining all other sources of noise to a minimum. The different sections of the protocol present technical and experimental procedures aimed at obtaining the best possible spatiotemporal resolution by limiting background noise, increasing the light output of the luciferase (see sections on donors and substrates above), improving the separation between donor and acceptor signals (see section on acceptors above), optimizing the light transmission of microscope optics and finally increasing the sensitivity of the detector. These latter aspects are discussed below.

Microscope setup

There are several bioluminescence imaging systems currently available on the market. These include the Olympus LV200 and the Atto Cellgraph. These systems are designed to minimize the

contamination by external light during measurements, thus increasing the SNR. When combined with adequate objective lenses and sensitive cameras, these systems offer excellent performance. However, most wide-field microscope setups equipped with a highly sensitive camera should be amenable to performing BRET microscopy with limited modifications. Although the images collected for this report were obtained using a regular inverted microscope, more sophisticated microscopes equipped for photoactivated localization microscopy (PALM), stochastic optical reconstruction microscopy (STORM), total internal reflection fluorescence (TIRF) or calcium imaging should also be suitable for BRET microscopy.

To minimize the contaminating lights (background noise), the imaging equipment should be placed in a dark room, and the system should be further shielded from stray light by inserting the microscope into a dark box covering the microscope body. All openings of the dark box should be covered by dark seals hermetic to light. All the light from the equipment within the dark box should be turned off or masked, and the use of light-emitting devices in the dark room should be minimal. All illumination sources (pilot lamps and indicators) in the dark room should be masked, except for a maximally dimmed computer screen needed for monitoring the image during the acquisition. To verify the influence of external light, images obtained in the absence of sample with the camera shutter closed should be compared to those obtained when the shutter is open. When comparing mean signal intensity between these two acquisitions, differences of ≤1 photon per pixel per min should be targeted using a non-amplified camera or EMCCD in photon-counting mode.

The microscope should be equipped with objective lenses having high light-collecting capacity. The image brightness is known to be influenced by three objective lens parameters: transmission (TR), numerical aperture (NA) and magnification (M), and is determined by the following formula:

$$(\text{Image brightness}) \propto \text{TR} \times \frac{(\text{NA})^2}{(M)^2}.$$

Therefore, they are the most important parameters to consider in selecting an objective lens for BRET imaging. Optimal lens magnification (M) is dependent on the surface area of the detector used. We usually combine a ×60 or ×100 lens with a 13 × 13-mm detector. It should be noted that sample brightness using a ×100 lens is ~30% of that obtained with a ×60 lens. The objective lens should be an oil immersion or water immersion lens having the highest available NA. Most high-quality objective lenses have high light transmission (TR) properties across the entire visible light spectrum. However, some lenses may have lower transmission in BRET2 assays, which emits violet light, which is at the lower edge of the visible spectrum. However, this limitation can be partly solved using lenses specifically designed for fluorescence measurement, because they tend to have higher transmission in the UV–violet range. The ×100 objective lens that we are using for BRET imaging (CFI Apochromat TIRF, Nikon) has a TR that drops from 82% at 510 nm to 48% at 400 nm. The relative transmission efficacy of the lenses can vary substantially between lens types and should be evaluated to select the best ones for the BRET pairs used as a function of the wavelength to be monitored.

Detector

Owing to the low signal, BRET imaging requires very sensitive cameras. The detection sensitivity of the camera is mainly determined by two parameters: (i) the quantum efficiency (QE) and (ii) the pixel size of the detector. In many scientific cameras, the peak QE at 500–600 nm is very high (80–90%), but drops rapidly to 10–60% in the UV–violet range, greatly compromising the detection sensitivity and thus the quality of the images when using a short-wavelength donor or acceptor. This is of particular concern for BRET2 assays, which require imaging of 400-nm violet signals originating from the luminescent donor. Therefore, the spectral response of the camera should be examined very carefully to select its QE characteristics as a function of the type of BRET imaging assay considered. The pixel size is the surface area of a single pixel on the sensor unit. Depending on the camera, it may range from 5 × 5 μm to 24 × 24 μm. The larger surface area has more chances to catch a photon, and improves the signal captured per pixel. Cameras having binning functions can bundle several pixels and treat the signal as if it were originating from a single pixel. Although larger pixels allow the detection of lower signals, making the camera more sensitive, it results in a lower-resolution image. The choice of a given pixel size is therefore always a compromise between sensitivity and resolution. We usually use a 170-μm^2 (13 × 13 μm) or 680-μm^2 (26 × 26 μm, 2 × 2 binning of 13 × 13 μm) pixel surface area using an EMCCD or CCD camera, respectively. Ideally, the size of the detector chip used should be ~13 × 13 mm (1,024 × 1,024 pixels of 13 × 13-μm pixels). This is based on the standard

Table 1 | Comparison of the noise level between cooled CCD and EMCCD cameras

	Cooled CCD camera Pixis 1024, Princeton Instruments		EMCCD camera EM N2, Nuvu cameras (photon-counting gain, 3,000)		EMCCD camera EM N2, Nuvu cameras (conventional gain, 500)	
	Average counts (e$^-$)	Noise level (r.m.s.)	Average counts (e$^-$)	Noise level (r.m.s.)	Average counts (e$^-$)	Noise level (r.m.s.)
Shutter closed	NA	6.90	NA	1.07	NA	295.82
Low signal	1.27	5.18	0.63	1.34	8.91	166.06
High signal	154.42	13.73	146.34	11.42	5,060.35	641.58

Each row represents image noise level in typical measurement conditions. Each image is exposed for 1 min, and signal statistics are calculated from 100 × 100 = 10,000 pixels cropped from the area having uniform illumination and not affected by the objective lens halo. Shutter closed: camera dark current when closing the camera shutter before CCD. Low signal: signal level close to the dark area of a typical luminescence-imaging picture capturing the system noise by exposing for a long time without a luminescent sample while opening the camera shutter. High signal: signal level close to a bright area of a luminescence-imaging picture obtained by introducing stray light so that the background signal is close to the typical input level from bright pixels of BRET measurement. r.m.s., root mean square.

field of view (FOV) of the microscope (18 mm). Depending on the combination of microscope system and objective lens, larger detector chips might be used without overfilling the FOV.

The typical signal detected in BRET imaging is a couple of photons per pixel per second (1–10 e$^-$/pixel/s) in our system. To limit the impact of the shot noise to a reasonably low level (<10 dB), we usually adjust exposure time so that the area of interest from the image corresponds to at least 100 photons captured per pixel. In addition to shot noise, another type of noise reducing image quality is known as 'thermal noise' or 'dark current' and corresponds to the random signal generated by thermal electrons produced by the camera itself. To reduce the thermal noise, the camera should be equipped with a cooling unit. In deep-cooled (typically below −60 °C) cameras, thermal noise is usually <0.01 e$^-$/pixel/s, which is small enough for good BRET imaging. For the images presented in this report, we used either thermoelectric cooling (Pixis camera) or liquid-nitrogen cooling (NuVu camera).

The final distinguishing factor between cameras is the 'readout noise', which originates from the signal processing of the camera circuit. EMCCD cameras are becoming increasingly popular for low-light imaging because they have a lower readout noise relative to the signal. This is achieved by amplifying the photoelectron signals with high gain. However, the multiplication process of EMCCD cameras also amplifies other sources of noise[62]; it is therefore recommended to use an EMCCD camera in photon-counting mode[63] in order to mitigate this negative effect of the high-gain amplification. Using a photon-counting strategy is also useful in minimizing the impact of cosmic rays on the image. Indeed, because the photon-counting image is generated as an integration of many (500–1,000) binary images with very short exposure, the high-energy signal from the cosmic ray is treated as a single-photon entry and therefore is diluted in the entire integrated image. Table 1 shows the comparison of the total noise level between CCDs and EMCCDs used in photon-counting mode or conventional mode. When the signal is strong enough, the noise level is similar between the two types of camera, independent of the detection mode because it reflects mainly the shot noise. By contrast, when the signal is very low, an EMCCD in photon-counting mode shows a much lower noise level than a CCD or an EMCCD in conventional mode. As a result, an EMCCD in photon-counting mode has a lower detection limit. This probably reflects the stochastic noise known as excess noise factor[62]. Photon counting is, indeed, known to be an effective way to reduce such noise in low-light condition[63]. Another advantage of EMCCD photon-counting mode over the conventional electron-multiplying (EM) mode results from the less detrimental influence of baseline signal drift that is sometimes observed as a function of imaging time, because the threshold used for photon counting is substantially higher than the baseline signal.

An EMCCD is also preferable to a CCD when short exposure times are required, as in the case of real-time imaging. This is well illustrated in Fig. 6a, where a weak luminescent signal could be detected for exposure times as short as 0.1–0.2 s using an EMCCD camera, but could not be detected with an exposure time <0.5–1.0 s with a CCD. Yet when the signal is of sufficient intensity, good-quality images can be obtained with both CCDs and EMCCDs. Indeed, Fig. 6b shows that the BRET between the G-protein subunits Gαq-RlucII and GFP10-Gγ1 expressed at the cell surface of HEK293 cells could be readily imaged with both cameras.
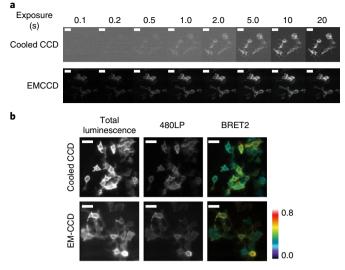
Fig. 6 | Comparison between cooled CCD and EMCCD camera. a, Comparison of luminescence images of cells expressing β-arrestin-RlucII using cooled CCD and EMCCD cameras. Each image frame is a monochrome gradation calibrated between 5 and 95% of maximal signal intensity. Scale bars, 20 μm. **b**, BRET2 images obtained using cooled CCD and EMCCD cameras. HEK293 cells were transfected with AT1R, Gαq-RlucII, Gβ1 and GFP10-Gγ1. BRET level was expressed as a heat map color code as described in Fig. 4a. The pixel brightness represents total photon counts of each pixel. Note: the bottom three pictures in **b** are derived from the same field of cells as those in Fig. 7a, but were taken at different time points and include more cells. Scale bars, 40 μm. 480LP, 480-nm longpass filter.

On the basis of these observations, we recommend an EMCCD camera with photon-counting mode as the preferred detector system for BRET imaging. However, it should be noted that photon counting narrows the linear range of quantification. Therefore, when the number of photons per pixel is >0.5 per image, counting becomes inaccurate as compared with that of other methods[63]. Therefore, exposure time should be adjusted in order to avoid signal saturation.

Materials

Biological materials
Cells of interest. In this example, we use HEK293T cultured human embryonic kidney cells (American Type Cell Culture Collection (ATCC), cat. no. CRL-3216). The use of this protocol is not limited to HEK293T cells; any other cell type that can express sufficient levels of luciferase- and GFP-fused constructs can be used. **!CAUTION** The cell lines used in your research should be regularly checked to ensure that they are authentic and are not infected with mycoplasma.

Reagents
▲ **CRITICAL** Although the suppliers used for all listed reagents are provided, alternatives exist in most cases. None of the reagents are harmful as long as they are handled according to general laboratory practice.
- DMEM (Wisent, cat. no. 319-015-CL)
- FBS (Wisent., cat. no. 080150)
- Penicillin–streptomycin mixture (Wisent, cat. no. 450-201-EL)
- Trypsin–EDTA mixture (Wisent, cat. no. 325-542-EL)
- DPBS (Wisent, cat. no. 211-410-XK)
- X-treme GENE 9 DNA transfection reagent (Roche Diagnostics, cat. no. 06365787001)
- Sodium chloride (NaCl; Laboratoire MAT, cat. no. SR-0091)
- Potassium chloride (KCl; Sigma, cat. no. P9541)
- Potassium dihydrogen phosphate (KH_2PO_4; Sigma, cat. no. P5379)
- Disodium hydrogen phosphate (Na_2HPO_4; Sigma, cat. no. S0876)
- Calcium dichloride ($CaCl_2$; Sigma, cat. no. C7902)
- Magnesium dichloride ($MgCl_2$; Laboratoire MAT, cat. no. MR-0103)
- HEPES (Sigma, cat. no. H4034)

• Anhydrous ethanol (Greenfield Specialty Alcohols, cat. no. P016EAAN)
• Molecular sieves (4 Å; Sigma, cat. no. M2635)

Luciferase substrates

▲ CRITICAL Luciferase substrates (CTZh, CTZ400a, Me-O-e-CTZ, Me-O-CTZ-O-Me and furimazine from a Nano-Glo Luciferase Assay Kit) are light sensitive and unstable in aqueous solutions. Solutions should be prepared as described in the 'Reagent setup' section.
• Coelenterazine h (CTZh; NanoLight Technology, cat. no. 301)
• Coelenterazine 400a (CTZ400a; NanoLight Technology, cat. no. 340)
• Methoxy e-CTZ (Me-O-e-CTZ/Prolume Purple; NanoLight Technology, cat. no. 369)
• Methoxy CTZ-methoxy (Me-O-CTZ-O-Me/Prolume Purple II; NanoLight Technology, cat. no. 367)
• NanoFuel solvent (NanoLight Technology, cat. no. 399)
• Nano-Glo Luciferase Assay Kit (Promega, cat. no. N1110)

Equipment

Cell culture

• 75-cm^2 Cell culture flasks (Falcon, cat. no. 353136)
• 35-mm Glass-bottom poly-D-lysine-coated culture dishes (Mattek, cat. no. P35GC-1.5-14-C)
• 15-ml Centrifuge tubes (Falcon, cat. no. 352096)
• 50-ml Centrifuge tubes (Falcon, cat. no. 352070)
• 1.5-ml Microcentrifuge tubes (Sarstedt, cat. no. 72.706)
• Cell incubator (37 °C, 5% (vol/vol) CO_2; Kendro, Heraus model no. HERAcell 150)
• Biological safety cabinet (Kendro, Heraus model no. HERAsafe HS12)
• Refrigerators (4 °C and −20 °C; Frigidaire, model no. MRT18DNCW0)

BRET imaging

• Inverted microscope (Nikon, model no. Eclipse Ti-U)
• EMCCD camera (NüVü Cameras, model no. EM N2)
• Objective lens (Nikon CFI Apochromat TIRF, 60× oil, NA 1.49)
• Objective lens (Nikon CFI Apochromat TIRF, 100× oil, NA 1.49)
• Cooled CCD camera (Princeton Instruments, model no. Pixis 1024B)
• Optical filter changer (Sutter Instruments; model no. Lambda 10-2) ▲ CRITICAL The motorized filter wheel of the Lambda filter changer has an IR LED inside the filter wheel for filter turret positioning, and this can be a possible source of light contamination. The Lambda filter changer can be modified by the manufacturer to allow turning off the LED during measurement. Alternatively, you can install an IR-blocking filter in front of the camera.
• Optical filters (550/80 nm for BRET1, 480-nm longpass for BRET2 and 550-nm longpass for Nluc with CyOFP or CyRFP, 25-mm diameter)
• Motorized focus controller (Prior, model no. Proscan)
• Microscope epi-fluorescence illumination source (470-nm LED; Thorlabs, cat. no. M470L3)
• Digital input/output (I/O) interface (National Instruments, cat. no. USB-6501)
• MetaMorph v.7.8 data acquisition software (Molecular Devices: https://www.moleculardevices.com/products/cellular-imaging-systems/acquisition-and-analysis-software/metamorph-microscopy#gref)
  ▲ CRITICAL In our experiments, all microscope hardware is controlled using MetaMorph v.7.8, but other instrument-control software (such as LabVIEW, MATLAB or LabWindows) can be equally used.
  ▲ CRITICAL The image analyses presented were performed using MetaMorph v.7.8. However, most analysis software that supports color mapping and image arithmetic processing (such as ImageJ or MATLAB) can be used.
• Computer system: Windows 7. The system should be equipped with enough PCI card slots, USB ports and serial ports depending on the devices connected to the microscope.

Reagent setup

Cell culture

In the example described in this protocol (HEK293T cells), the cell culture medium is DMEM supplemented with 10% (vol/vol) FBS, 1% (vol/vol) penicillin–streptomycin solution. Cell culture medium can be stored at 4 °C for up to 4 weeks, not exceeding the expiration date of the medium. Maintain HEK293 cells at 37 °C in 5% (vol/vol) CO_2. On the basis of a doubling time of ~20 h, cells

should be split in a 1:10–1:20 (vol/vol) ratio twice a week, using a trypsin–EDTA solution to detach the cells.

Modified Hank's balanced salt solution

Prepare the following solution as a 10× concentrated stock: 1.379 M NaCl, 53.3 mM KCl, 4.4 mM KH_2PO_4 and 3.3 mM Na_2HPO_4. The 10× stock solution can be stored at room temperature (21 ± 2 °C) for up to 12 months. Freshly prepare 1× solution and add 1 mM $CaCl_2$, 1 mM $MgCl_2$ and 10 mM HEPES, pH 7.4, on the day of the experiment.

Substrate (CTZ) solution

Dissolve CTZh and CTZ400A in anhydrous ethanol to generate 1 mM stock solutions. The ethanol used to dilute the CTZs should be made completely anhydrous by adding 4-Å molecular sieves. Dissolve Me-O-e-CTZ and Me-O-CTZ-O-Me in NanoFuel solvent to generate 2 mM stock solutions. Dilute furimazine from the Nano-Glo Luciferase Assay Kit with the buffer provided with the kit. All substrate solutions can be stored desiccated, in the dark at −20 °C for up to 1 month. Prepare the diluted working concentrations immediately before use.

Equipment setup

Detectors

We recommend an EMCCD camera using photon-counting acquisition mode. However, other types of deep-cooling cameras can also be used (see 'Detector' in the 'Experimental design' section above).

Cultureware

We use poly-D-lysine-coated culture dishes for BRET imaging. This is because the attachment of HEK293 cells to glass is weak, and cells can detach from the culture surface during washing or treatment steps. Other surface treatments can be used if they provide sufficient cell attachment. The thickness and material of the culture surface should be compatible with the specifications of the objective lens used. Usually, objectives are designed to be used with a cover glass of 0.17-mm thickness, and we recommend using no. 1.5-thickness (0.16–0.19-mm) glass-bottom cultureware. We use commercially available pre-coated cultureware. Alternatively, culture dishes can be coated in the laboratory, using cell culture–grade 0.1 mg/ml poly-D-lysine solution. In that case, the bottoms of the dishes should be covered with 1 ml of poly-D-lysine solution for at least 1 h, and then washed twice with 2 ml of dH_2O just before use.

Optical filters

Adequate filter pairs for the BRET donor and acceptor must be installed in a filter wheel that allows rapid exchange between filters (see 'Equipment' section for a description). The filters to be installed vary according to the BRET configuration used. Filters typically used for BRET1, BRET2 and Nluc-BRET assays are listed in the 'Equipment' section. Because BRET can be calculated by dividing the signal detected in the acceptor channel by the total luminescence, the donor filter position can be left empty.

Microscope hardware connection

The imaging device (EMCCD camera or cooled CCD camera) requires a fast connection, such as Camera Link, GigE Vision or USB2/3. However, because BRET/luminescence microscopy requires a long exposure time, other devices (e.g., filter wheels, focus controller, illumination) do not require very precise timing and can be controlled through conventional serial ports or transistor–transistor logic (TTL) outputs. In our setup, the EMCCD camera is connected to the computer with a Camera Link frame grabber board supplied by the camera manufacturer. A cooled CCD camera is connected via USB2. The optical filter changer and motorized focus controller are connected using serial ports. Epi-fluorescence and bright-field illuminations are controlled through TTL switches or power relays accepting TTL inputs to prevent accidental activation during luminescence measurements.

Procedure

Cell preparation ● Timing ~74 h

1. 3 d before imaging, seed 1×10^5–3×10^5 HEK293T cells into 35-mm poly-D-lysine-coated glass-bottom culture dishes ('Equipment setup') in 2 ml of fresh medium. Incubate the cells at 37 °C in 5% (vol/vol) CO_2 for 24 h.

> **Box 1 | Determination of donor to acceptor ratio** ● Timing ~74 h for cell preparation and 1 h for measurement
>
> When monitoring intermolecular BRET (for instance, when monitoring protein–protein interactions or translocation of a protein from one compartment to another), the expression levels of the donor and acceptor affect the BRET signal. The ideal donor/acceptor ratio depends on the apparent affinity between the donor- and acceptor-fused components and the experimental design considered. To determine the best donor/acceptor ratio for a given experimental setting, we use the following procedure.
>
> **Procedure**
> ▲ CRITICAL Although this determination can be performed in imaging mode, it is easier and faster to do it by spectrophotometry using PMT-based plate readers[7]. The ratios determined this way are generally a good indication of the ratios that should be used for BRET imaging.
> 1 Express the donor- and the acceptor-fused components individually in the target cells of interest.
> 2 Determine the range of the DNA amount for which the luminescence and the fluorescence signals are quantifiable but do not affect the viability or morphology of the cells. In addition, make sure that the subcellular distribution of the tagged proteins is not affected by the expression levels.
> 3 Using the lowest amount of DNA yielding a detectable signal for the donor-fused component, perform an acceptor titration experiment by co-transfecting increasing amounts of the acceptor-fused component (within the range determined in step 2).
>   ▲ CRITICAL STEP This is important in order to avoid excessive overexpression, which could lead to spurious interactions. If possible, it is good practice to quantify the BRET probe expression levels to confirm that it remains close to physiological conditions. The BRET signal will increase as a function of the ratio of the acceptor to the donor until the donor is saturated by the acceptor.
> Depending on the experimental design (monitoring a phenomenon that should lead to an increase or decrease in BRET), select the ratio that will provide the largest BRET change window.

2   2 d before imaging, transfect the cells with the Luc-tagged BRET donor and GFP-tagged BRET acceptor. For each dish, dilute 3 µl of X-treme GENE 9 DNA transfection reagent with 100 µl of FBS-free culture medium and mix with a total of 1 µg of DNA in an Eppendorf tube. Vortex and add dropwise to the cells. Incubate the cells at 37 °C in 5% (vol/vol) CO_2 for 48 h.
    ▲ CRITICAL STEP The ratio of expression between the BRET donor and acceptor can critically affect the BRET signal level. See Box 1 for guidance on how to determine the adequate donor/acceptor ratio.

3   (Optional) If the aim is to test the effect of pretreatment with a drug of interest, add the drug or the vehicle (used as control) to a well of the glass-bottom culture dish and incubate the cells at 37 °C in the cell culture incubator for the time of the treatment (see 'Anticipated results').
    ▲ CRITICAL STEP Some drugs may have physicochemical properties (e.g., pH, ionic strength, color, red-ox activity) that may interfere with the luciferase signal, either by affecting the enzyme activity or by having optical properties that affect the readings (e.g., quenching, autofluorescence). To control for these potentially artifactual effects, the impact of the drug treatment is tested on the signal from the luciferase expressed alone and/or on a control fusion protein linking the energy donor to the acceptor. If the drug treatment substantially affects either the luminescence signal or the BRET signal from the control fusion protein, such treatment should be avoided.

BRET image acquisition using an EMCCD camera ● Timing 1 h for setup + 10–120 min per dish for acquisition

4   Turn on the microscope system and launch the image acquisition software. Set the cooling temperature of the camera.
    ! CAUTION We use a liquid-nitrogen–cooled camera. If such a cooling system is used, the ventilation of the microscope room should be verified before starting to fill the liquid nitrogen tank. Most of the deep-cooling cameras on the market are equipped with a Peltier (thermoelectric) cooler.

5   After the camera temperature has reached −85 °C, set the EM gain. We usually use a calibrated EM gain of 3,000.
    ▲ CRITICAL STEP Monitor the camera temperature and wait until the sensor unit is fully cooled and stabilized. The reading should be performed at a camera temperature that minimizes dark noise caused by thermally generated electrons. For our camera, −85 °C was selected.
    ▲ CRITICAL STEP The 3,000 EM-gain value is used for our camera (NüVü EM N2). If a different EMCCD camera is used in photon-counting mode, the EM gain should be set to the maximal value for the specific camera used. For an intensified CCD or EMCCD in conventional acquisition mode, the amplification gain should be determined to maximize SNR.

6　Obtain a dark image: turn off all microscope illumination and room lighting. Close the microscope dark box. Set the EMCCD camera to photon-counting mode. Send a command to the filter changer and remove the filter in front of the camera. To confirm that there is no external light contaminating the image, set the exposure time to 0.1 s and repeat 100–200 successive photon-counting measurements without filters. Integrate all photon counts for each pixel and generate one image without mounting samples. All pixel values should be close to zero and show only uniform white noise.

▲ CRITICAL STEP　Make sure to turn off all illumination before activating the camera. Exposing the EMCCD to excessive light can damage the imaging unit.

▲ CRITICAL STEP　To acquire an image in non-photon-counting mode, using either a cooled CCD camera or the EMCCD camera, the same procedure can be used, but because of the lower sensitivity of the camera, longer exposure times are required to obtain images with sufficient SNR and resolution. In addition, because the dynamic range in non-photon-counting mode is wider, there is no need to obtain multiple frames of the same images, and therefore integration of multiple images is not required. In that case, we set the total exposure time so that the signal strength of the area of interest is at least five to ten times higher than the noise level root mean square of a blank image having the identical exposure time. These comments also apply to Steps 10–13.

? TROUBLESHOOTING

7　After confirming that the camera has stopped recording, turn on the room lighting and remove one culture dish (from Step 2) from the cell incubator. Remove the cell culture medium, wash the cells once with 1 ml of modified Hank's balanced salt solution (HBSS) and remove the modified HBSS without drying the cells. For long time-course experiments, phenol red–free culture medium can be used instead of modified HBSS in order to minimize morphological and physiological changes. However, it should be noted that we obtain a weaker signal strength and higher background in culture medium versus modified HBSS, most likely due to some form of quenching and spontaneous oxidation of the substrates.

8　Open the dark box and mount the dish on the microscope. Focus on a field of cells, using bright-field or epi-fluorescence illumination.

9　Add 500 µl of modified HBSS containing an adequate amount of luciferase substrate. We typically use 10–20 µM CTZh for BRET1 and 10–20 µM Me-O-e-CTZ for BRET2 and ebBRET measurements. We use 10–20 µM CTZ400a for the Nluc and CyOFP/CyRFP BRET pair.

10　Set up the focus (image preview): turn off all microscope illumination and room lighting. Close the dark box. Set the image exposure time to 0.1 s and obtain five frames without a filter. Generate an image by integrating the photon counts from the five frames. Continuously generate images and, on the basis of these coarse images, move the microscope stage and focus on the cells of interest (i.e., luminescent cells). Stop recording when focusing is finished.

▲ CRITICAL STEP　This step describes our default setting for an EMCCD camera in photon-counting mode. For other types of cameras, simply start live imaging with adequate exposure time according to the sensitivity of the camera. Typically, a non-amplifying camera requires 5–10 s of exposure to obtain luminescence images.

▲ CRITICAL STEP　Make sure to turn off all illuminations before activating the camera. Exposing the EMCCD camera to excessive light can damage the signal multiplier.

11　Generate the BRET image: set the exposure time to 0.1 s. Obtain 100 photon-counting frames without a filter and generate the total (donor and acceptor) luminescence image. Then send a command to the filter changer to insert the acceptor filter (corresponding to the acceptor emission bandwidth, 480-nm longpass in the case of BRET2; see 'Equipment' section for a complete list). Wait until the filter wheel stops moving (~0.1 s, depending on wheel model and position of filters). Obtain another 100 frames and generate the acceptor luminescence image; then remove the acceptor filter, again using the filter changer. The acquisition of the two images takes ~25 s. Repeat acquisition of the two images (100 photon-counting frames at a time) until the total photon count of the pixels in the region of interest reaches ~100 counts. Typically, ten cycles (1,000 frames each for total and acceptor) of acquisition will be required to obtain high-quality images.

▲ CRITICAL STEP　To maximize the number of photons collected to optimize the image quality, we recommend not using filters during the first (donor) measurement and calculating BRET as a ratio between acceptor emissions and total luminescence. However, BRET can also be calculated as a ratio of acceptor emissions to donor emissions, if a filter corresponding to donor wavelength is used during the first measurement.

▲ **CRITICAL STEP** This step describes our default setting for the EMCCD camera in photon-counting mode. For other types of cameras, capture a single image with adequate exposure time according to the sensitivity of the camera.

▲ **CRITICAL STEP** The linearity of the measurement can be affected if any given pixel is saturated (i.e., if one pixel is excited by more than one photon). To avoid such inaccurate photon counting, we recommend selecting exposure times that lead to the detection of any given pixel in <50 frames out of 100 frames[63].

(Optional) Time-lapse recording ● Timing variable, depending on the experimental design

12   To assess the dynamics of the process being imaged, perform time-lapse imaging by repeating Step 11 several times.

▲ **CRITICAL STEP** Although the light signal originating from luciferase decays over time, the BRET values will still be valid because it is a ratiometric measurement. However, a minimal luminescence signal is required to maintain image quality. The minimum signal strength required for proper image analysis may differ for different subcellular compartments but generally must be between 25 and 100 counts per pixel over 1,000 frames. Because different substrate/luminescent enzyme pairs have different brightness and time decays (Figs. 3 and 5), the time of continued imaging will vary according to the BRET configuration used.

13   (Optional) When the aim is to monitor the real-time effect of drug treatments, add the drug of interest after 5 min of time-lapse imaging, manually adding the drug in an additional 500 μl of modified HBSS and continuing imaging for 15–30 min (see 'Anticipated results').

Image analysis ● Timing 1–2 h

14   Launch the image analysis software and open the total luminescence images for all acquired frames. Select the image of interest and integrate the photon counts for each pixel, using the arithmetic/addition function of MetaMorph. Open time-matching acceptor images and integrate the photon counts for each pixel, using the same arithmetic/addition function. Save as integrated total (A) and acceptor (B) images, respectively.

15   Calculate the BRET ratio for each pixel. In the case of MetaMorph, use the arithmetic/divide function with the following formula:

$$(\text{Ratiometric image}(C)) = (\text{acceptor count image}(B)) \times 1,000/(\text{total count image}(A)).$$

For other software, divide the signal level of B by A and multiply by 1,000 for all corresponding pixels. A multiplication factor of 1,000 is used because most image analysis software (including MetaMorph) cannot handle values <1 that result from the division.

▲ **CRITICAL STEP** Note that the pixel values calculated here are affected by the differences in camera sensitivity (QE) and optical transparency between the two channels (total versus acceptor). Because microscopy systems (cameras and lenses) usually have lower sensitivity for BRET2 donor luminescence (400 nm) as compared with donors of longer wavelengths, the pixel value may not reflect the real ratio of the number of photons released. It follows that the calculated BRET values will be different from those obtained using spectrometric systems with photomultiplier tubes (PMTs). Yet, as long as the measurements do not fall outside the linearity range of the camera, the image BRET values are proportional to the real transfer and thus can be quantitatively compared with one another.

▲ **CRITICAL STEP** To obtain good-quality BRET images that can be reliably quantified, we calculate BRET as the ratio of the light emitted in the acceptor channel divided by the total luminescence detected, instead of the ratio of light emitted in the acceptor channel to that in the donor channel, which is generally used in spectrometric BRET measurements. The reason for using the total luminescence as the denominator of the ratio is that, in ebBRET in particular, the transfer of energy is extremely efficient, yielding to important decreases in the light emitted in the donor channel, rendering the donor signal more susceptible to noise factors. In addition, the reduced donor signal left after transfer can be too low for proper imaging, decreasing the sensitivity of the assay and increasing the variability. By contrast, using the total luminescence signal as the denominator provides reliable ratiometric values, for which robustness is not affected by the extent of transfer.

16   Assign a heat map to the ratiometric image (C). For the analysis with MetaMorph, set the lookup table (LUT) mode to pseudocolor and adjust the color scale so that all interesting regions are within the range of the pseudocolor rainbow hue, without saturation. Typically, we set 0 to purple

(lowest signal) and 800 to red (highest signal). For time-lapse experiments, apply a heat map having the same signal range to all frames. Convert the image to an RGB image (24 bit/pixel TIFF) and save as the raw BRET image (D).

17 Open the total luminescence image (A). Scale the image so that the image grayscale covers the entire image, using the 0.5% brightest pixels as white and the 0.5% darkest pixels as black. Convert the image to an 8-bit/pixel monochrome TIFF and save as a signal strength image (E).

18 Correct the raw BRET image (D) as a function of the signal strength image (E) for each pixel. Because a 24-bit/pixel TIFF has 8-bit depth for the red, green and blue channels, calculation in MetaMorph is as follows:

(raw BRET (D)) × (signal strength (E))/256.

For other software, multiply each pixel value of the R, G, and B planes of image (D) by the value of the corresponding pixel from image (E) and divide by 256. The resulting image shows the BRET signal level of each pixel.

19 (Optional) If quantification of BRET signals originating from different cell compartments is required, a mask corresponding to the ROI must be prepared; total photon counts from the donor and acceptor within each of the ROIs should be integrated, and BRET should be calculated as presented in Supplementary Data 1.

Troubleshooting

Step 6: background signal and contaminating light

If the camera does not have a function to subtract pixel bias (resulting from the variability of the individual detector sensitivity in the camera detector array) automatically, a 'bias image' also known as a 'bias frame' must be generated manually under no-illumination conditions. Prepare the bias image using the following procedure:

Close the camera shutter.

Set the exposure time to zero or a very small value. Obtain five to ten images.

Generate the bias image by calculating medians of each pixel, using all captured images.

The bias image should be subtracted from all following images. To remove the influence of sporadic high-energy artifacts (e.g., cosmic rays), the bias image should be generated using the medians and not the average of each pixel for the five to ten images obtained.

If the source of the contaminating signal remains after the bias subtraction, this can have a number of causes:

Light contamination: block the light source causing the contamination. The motorized microscope components using IR LEDs to adjust the position of the moving parts may also cause interference. Turn off the IR LEDs when not in use or use a filter to block the light.

Elevated camera dark current: check if the cooling system of the CCD is working correctly and adjust appropriately.

Cosmic rays: these classically cause bright dots or lines showing up randomly on the image. It is not practical to shield for the cosmic rays because they have very high energy. Photon-counting measurement with an EMCCD, as compared with the traditional imaging mode, markedly decreases the contribution of cosmic rays. When using non-photon-counting mode for image acquisition, the best way to remove the influence of cosmic rays is to capture five to ten images and to generate the final image by calculating the median values and not the average for each pixel.

Auto-oxidation of substrates: CTZs are unstable in aqueous solutions and emit light by auto-oxidization. The auto-oxidation of the substrate is observed as a uniform increase of the background signal. The increase is relatively low when modified HBSS is used as the assay medium. However, it might be problematic for other assay media, such as serum-containing medium.

Timing

Steps 1–3, cell preparation: 30 min of seeding cells + 24 h of incubation + 1 h for transfection + 48 h of incubation

Steps 4–11, BRET image acquisition using an EMCCD camera: 1 h for setup + 10–120 min per dish, depending on the experimental design

Steps 12 and 13, (optional) time-lapse recording: variable, depending on the experimental design

Steps 14–19, image analysis: 1–2 h

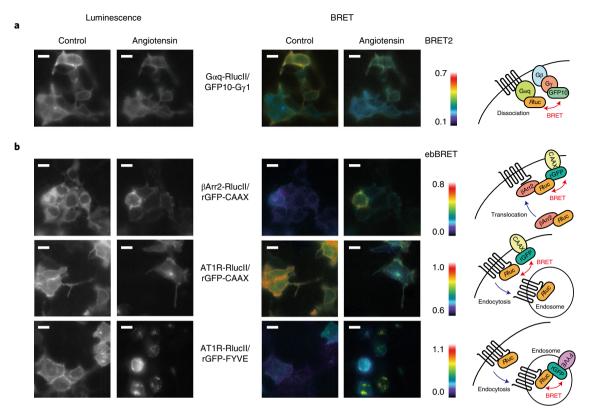Box 1, determination of donor to acceptor ratio: ~74 h for cell preparation + 1 h for measurement

Fig. 7 | Examples of BRET imaging in GPCR signaling. a, BRET2 imaging. Dissociation of G-protein α subunit from βγ complex upon GPCR activation. HEK293 cells were transfected with AT1R, Gαq-RlucII (RlucII is inserted at position 118 of Gαq), Gβ1 and GFP10-Gγ1. 10 μM Me-o-e-CTZ was added and BRET2 images were obtained before and after treatment with 100 nM angiotensin II (AT1R agonist) for 5 min. **b**, ebBRET imaging. Recruitment of β-arrestin to the plasma membrane and GPCR endocytosis. HEK293 cells were transfected with AT1R, β-arrestin2-RlucII and rGFP-CAAX (top panel), with AT1R-RlucII and rGFP-CAAX (middle panel), or with AT1R-RlucII and rGFP-FYVE (bottom panel). In the rGFP-CAAX construct, rGPF was linked with the CAAX box (GKKKKKKSKTKCVIM) using a 14-amino-acid linker (GSAGTMASNNTASG). In the rGFP-FYVE construct, rGFP was linked with the FYVE domain using an 11-amino-acid linker (GSGGGSGSGGLE). A 10 μM final concentration of Me-O-e-CTZ was added, and ebBRET images were obtained before (control) and after treatment with 100 nM angiotensin II for either 15 min (top panel) or 60 min (middle and bottom panels). In each image, the BRET level was expressed as a heat map color code as described in Fig. 4a. The pixel brightness represents the total photon count of each pixel. Scale bars, 20 μm. βArr2, β-arrestin2.

Anticipated results

Examples of BRET images that can be expected are provided in Figs. 4–7. A comparison of BRET image intensity obtained in three different BRET modes (BRET1, BRET2 and ebBRET) is presented in Fig. 4. The data were obtained with constructs genetically fusing the energy donor to the acceptor, providing excellent controls to test the imaging systems. Although ebBRET provides the brightest images, it cannot be used to monitor specific interactions between protein partners because it takes advantage of the self-assembly of Rluc and rGFP when they are present in the same compartment and could promote interactions between proteins that do not interact with one another normally. Thus, it is mainly suitable for monitoring translocation between compartments.

When comparing BRET1 and BRET2, although weaker luminescence is emitted in BRET2, the better separation of the acceptor and donor signals clearly increases the dynamic window of the BRET signal, allowing better imaging as compared to those produced with BRET1. This is illustrated in Fig. 4a, which shows images of total luminescence emitted (left panels), the light emitted by the acceptor (middle panels) and the calculated BRET signal (right panels) for cells expressing the donor alone (β-arrestin2-RlucII, rows 1 and 3) or a fusion between RlucII and Venus (BRET1; row 2) or GFP2 (BRET2; row 4) upon addition of CTZh (rows 1 and 2) or Me-O-e-CTZ (rows 3 and 4). As can be readily observed, a much greater background BRET signal is observed in BRET1 in the absence of acceptor (Fig. 4a, top row, right image and Fig. 4b, BRET1 donor only). This results from the overlap between the wide emission spectrum of Rluc and the emission of Venus, yielding a greater contamination of the donor emission signal in the acceptor channel (Fig. 4a, top row, middle image). A much lower background BRET is observed in BRET2. Because similar maximal BRET signals are
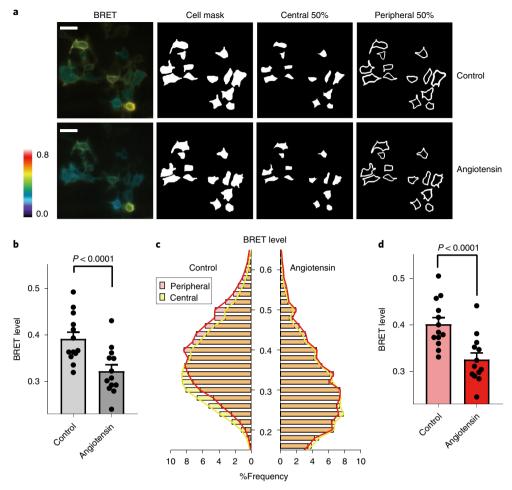
Fig. 8 | Example of image quantification. a, Image segmentation. Images used for analysis come from the experiment presented in Fig. 6b (bottom row) and 7a, before (top left column) and after (bottom left column) the treatment with angiotensin II. 13 cells showing high luminescence signals (>30–50 photons per pixel) were segmented manually (second column). Each cell area was divided into central (third column) and peripheral (fourth column) regions. These two regions have equal surface areas. BRET level was expressed using a heat map as described in Fig. 4a. Scale bars, 40 µm. **b**, Quantification of BRET level. BRET level of each cell before and after the stimulation was calculated from the sums of photon counts in each cell region according to the formula shown in Fig. 4. The bars represent the mean ± s.e.m. in the presence or absence of angiotensin II. *P* value was calculated by paired *t* test (two-tailed), *n* = 13. **c**, The distribution of BRET levels was expressed as histograms (left, control; right, angiotensin) for the central and peripheral regions of cells. The bin width of the histogram is equal to 0.02 arbitrary BRET values and is plotted against relative frequency for each bin. The difference of BRET level between the peripheral and central region was quantified using the same calculation as in **b**. **d**, The bars represent the mean ± s.e.m. of the BRET values calculated from peripheral regions of the cells in the presence or absence of angiotensin II. *P* value was calculated by paired *t* test (two-tailed), *n* = 13.

observed for BRET1 and BRET2 (Fig. 4b, donor + acceptor), the lower background results in a much greater dynamic BRET window (maximal/background signals) for BRET2 (6.5-fold in BRET2 versus 1.7 in BRET1) (Fig. 4b). It follows that, although BRET1 generates brighter and longer-lasting signals that can be useful for imaging proteins expressed at low levels for extended periods of time, the dynamic window offered by BRET2 allows better separation between background and specific signals (Fig. 4c), making it a better choice for imaging when the process studied leads to small differences in BRET signals. Also shown in Fig. 4 is the fact that the BRET dynamic window observed for ebBRET is larger than those of both BRET2 and BRET1, owing to the high transfer efficiency observed for this donor–acceptor pair, making it the best choice to monitor protein translocation (see below).

A wide range of biological processes can be imaged by different BRET modalities. For example, we used BRET2 to monitor the activation of a heterotrimeric G protein (Gαqβ1γ1) by AT1R (Fig. 7a). The separation between Gα and Gβγ can be detected by measuring the decrease in BRET signal between the Gαq tagged with RlucII and the Gγ tagged with GFP10 following the activation of the

receptor by angiotensin. This type of approach can be used to monitor the dynamic regulation of any protein–protein interaction. Both BRET increase and BRET decrease can be monitored, depending on the effect of a particular stimulus on the interaction. In Fig. 7b, we illustrate the use of ebBRET to image the subcellular redistribution of AT1R and the regulatory protein β-arrestin following activation with the AT1R agonist angiotensin-II. The translocation of β-arrestin to the plasma membrane upon receptor activation is visualized by monitoring the BRET between β-arrestin2-RlucII and rGFP tagged with a CAAX box from KRas (rGFP-CAAX)[64] that targets it to the plasma membrane (Fig. 7b, top panels). The ensuing agonist-promoted endocytosis of the receptor that occurs can also be detected by imaging ebBRET between AT1R-RlucII and rGFP targeted to either the plasma membrane (rGFP-CAAX) or the early endosomes, using the early endosome localization motif, FYVE from endofin[65] (Fig. 7b, middle and bottom panels, respectively). The use of rGFP selectively targeted to distinct subcellular organelles allows monitoring of the localization of an Rluc-tagged protein in these specific organelles. Here, examples for plasma membrane and endosome are provided, but similar experiments can be done for other compartments, such as endoplasmic reticulum, Golgi, nucleus, mitochondria.

The comparison between control and angiotensin-stimulated conditions for β-arrestin translocation (Fig. 7b, top panel) was done using the same cell population by taking images before and after treatment. This is possible because the recruitment of β-arrestin to the plasma membrane is relatively rapid following agonist treatment and thus can be monitored in real time before the luminescence signal decays to levels that compromise image quality. However, in the case of the receptor endocytosis (Fig. 7b, middle and bottom panels), the control and angiotensin conditions needed to be imaged in different cell populations because the luminescence signal decayed to levels incompatible with quality imaging before reliable endocytosis could be observed. It is important to note that statistically significant differences can be obtained between control and stimulated conditions, both when assessing the phenomenon in the same cell and when assessing it in different sets of cells (Supplementary Fig. 1).

Quantification of BRET signals in different subcellular compartments can also be achieved. This is illustrated in Fig. 8, which shows the dissociation of Gαq-Rluc from GFP10-Gγ1 upon stimulation of AT1R. For this purpose, bright cells from the FOV are manually segmented (Fig. 8a, cell mask), and the BRET is determined for each cell by dividing the light signal emitted in the acceptor channel by the total light detected. The individual BRET values for each cell are then averaged, and the values obtained under basal and receptor-stimulated conditions are compared. As shown in Fig. 8b, receptor stimulation leads to a statistically significant reduction in BRET. Next, the quantification is performed on a subcellular domain by dividing each cell area into peripheral and a central regions (Fig. 8a, central 50% and peripheral 50%) so as to isolate the signal largely originating from the plasma membrane. Figure 8c illustrates the distribution of pixel-by-pixel BRET levels for the population of cells in the FOV, expressed as histograms for both untreated and angiotensin-stimulated conditions. As can be seen, receptor activation leads to a reduction of the frequency of high BRET pixels. When considering only the signal coming from the periphery, receptor stimulation leads to a statistically significant reduction of the BRET signal (histogram in Fig. 8d), indicating that the receptor-promoted dissociation of Gαq-Rluc from GFP10-Gγ1 occurring at the cell surface can be detected and quantified. The raw image data, the cell masks and the MATLAB script used for this quantification are available as Supplementary Data 1.

Reporting Summary
Further information on research design is available in the Nature Research Reporting Summary.

Data availability
The authors declare that all data supporting the findings in this study are available from the corresponding author upon request.

References

1. Förster, T. Zwischenmolekulare energiewanderung und fluoreszenz. *Ann. Phys.* **437**, 55–75 (1948).
2. Jares-Erijman, E. A. & Jovin, T. M. FRET imaging. *Nat. Biotechnol.* **21**, 1387–1395 (2003).
3. Berney, C. & Danuser, G. FRET or no FRET: a quantitative comparison. *Biophys. J.* **84**, 3992–4010 (2003).
4. Angers, S. et al. Detection of beta 2-adrenergic receptor dimerization in living cells using bioluminescence resonance energy transfer (BRET). *Proc. Natl. Acad. Sci. USA* **97**, 3684–3689 (2000).

5. Xu, Y., Piston, D. W. & Johnson, C. H. A bioluminescence resonance energy transfer (BRET) system: application to interacting circadian clock proteins. *Proc. Natl. Acad. Sci. USA* **96**, 151–156 (1999).

6. Ayoub, M. A. et al. Monitoring of ligand-independent dimerization and ligand-induced conformational changes of melatonin receptors in living cells by bioluminescence resonance energy transfer. *J. Biol. Chem.* **277**, 21522–21528 (2002).

7. Mercier, J.-F., Salahpour, A., Angers, S., Breit, A. & Bouvier, M. Quantitative assessment of beta 1- and beta 2-adrenergic receptor homo- and heterodimerization by bioluminescence resonance energy transfer. *J. Biol. Chem.* **277**, 44925–44931 (2002).

8. Galés, C. et al. Real-time monitoring of receptor and G-protein interactions in living cells. *Nat. Methods* **2**, 177–184 (2005).

9. Galés, C. et al. Probing the activation-promoted structural rearrangements in preassembled receptor-G protein complexes. *Nat. Struct. Mol. Biol.* **13**, 778–786 (2006).

10. Kobayashi, H., Ogawa, K., Yao, R., Lichtarge, O. & Bouvier, M. Functional rescue of beta-adrenoceptor dimerization and trafficking by pharmacological chaperones. *Traffic* **10**, 1019–1033 (2009).

11. Hamdan, F. F., Audet, M., Garneau, P., Pelletier, J. & Bouvier, M. High-throughput screening of G protein-coupled receptor antagonists using a bioluminescence resonance energy transfer 1-based beta-arrestin2 recruitment assay. *J. Biomol. Screen.* **10**, 463–475 (2005).

12. Charest, P. G. & Bouvier, M. Palmitoylation of the V2 vasopressin receptor carboxyl tail enhances beta-arrestin recruitment leading to efficient receptor endocytosis and ERK1/2 activation. *J. Biol. Chem.* **278**, 41541–41551 (2003).

13. Terrillon, S., Barberis, C. & Bouvier, M. Heterodimerization of V1a and V2 vasopressin receptors determines the interaction with beta-arrestin and their trafficking patterns. *Proc. Natl. Acad. Sci. USA* **101**, 1548–1553 (2004).

14. Bertrand, L. et al. The BRET2/arrestin assay in stable recombinant cells: a platform to screen for compounds that interact with G protein-coupled receptors (GPCRS). *J. Recept. Signal Transduct. Res.* **22**, 533–541 (2002).

15. Azzi, M. et al. Beta-arrestin-mediated activation of MAPK by inverse agonists reveals distinct active conformations for G protein-coupled receptors. *Proc. Natl. Acad. Sci. USA* **100**, 11406–11411 (2003).

16. Héroux, M., Breton, B., Hogue, M. & Bouvier, M. Assembly and signaling of CRLR and RAMP1 complexes assessed by BRET. *Biochemistry* **46**, 7022–7033 (2007).

17. Perroy, J., Pontier, S., Charest, P. G., Aubry, M. & Bouvier, M. Real-time monitoring of ubiquitination in living cells by BRET. *Nat. Methods* **1**, 203–208 (2004).

18. Stoddart, L. A. et al. Application of BRET to monitor ligand binding to GPCRs. *Nat. Methods* **12**, 661–663 (2015).

19. Stoddart, L. A., Kilpatrick, L. E. & Hill, S. J. NanoBRET approaches to study ligand binding to GPCRs and RTKs. *Trends Pharmacol. Sci.* **39**, 136–147 (2018).

20. Loening, A. M., Fenn, T. D., Wu, A. M. & Gambhir, S. S. Consensus guided mutagenesis of *Renilla* luciferase yields enhanced stability and light output. *Protein Eng. Des. Sel.* **19**, 391–400 (2006).

21. Hall, M. P. et al. Engineered luciferase reporter from a deep sea shrimp utilizing a novel imidazopyrazinone substrate. *ACS Chem. Biol.* **7**, 1848–1857 (2012).

22. Xu, X. et al. Imaging protein interactions with bioluminescence resonance energy transfer (BRET) in plant and mammalian cells and tissues. *Proc. Natl. Acad. Sci. USA* **104**, 10264–10269 (2007).

23. Coulon, V. et al. Subcellular imaging of dynamic protein interactions by bioluminescence resonance energy transfer. *Biophys. J.* **94**, 1001–1009 (2008).

24. Kim, J. & Grailhe, R. Nanoluciferase signal brightness using furimazine substrates opens bioluminescence resonance energy transfer to widefield microscopy. *Cytometry A* **89**, 742–746 (2016).

25. Goyet, E., Bouquier, N., Ollendorff, V. & Perroy, J. Fast and high resolution single-cell BRET imaging. *Sci. Rep.* **6**, 28231 (2016).

26. Namkung, Y. et al. Monitoring G protein-coupled receptor and β-arrestin trafficking in live cells using enhanced bystander BRET. *Nat. Commun.* **7**, 12178 (2016).

27. Beautrait, A. et al. A new inhibitor of the β-arrestin/AP2 endocytic complex reveals interplay between GPCR internalization and signalling. *Nat. Commun.* **8**, 15054 (2017).

28. De, A., Ray, P., Loening, A. M. & Gambhir, S. S. BRET3: a red-shifted bioluminescence resonance energy transfer (BRET)-based integrated platform for imaging protein-protein interactions from single live cells and living animals. *FASEB J.* **23**, 2702–2709 (2009).

29. Yeh, H.-W. et al. Red-shifted luciferase-luciferin pairs for enhanced bioluminescence imaging. *Nat. Methods* **14**, 971–974 (2017).

30. Fredriksson, S. et al. Protein detection using proximity-dependent DNA ligation assays. *Nat. Biotechnol.* **20**, 473–477 (2002).

31. Kerppola, T. K. Visualization of molecular interactions by fluorescence complementation. *Nat. Rev. Mol. Cell Biol.* **7**, 449–456 (2006).

32. Pelletier, J. N., Campbell-Valois, F. X. & Michnick, S. W. Oligomerization domain-directed reassembly of active dihydrofolate reductase from rationally designed fragments. *Proc. Natl. Acad. Sci. USA* **95**, 12141–12146 (1998).

33. Ozawa, T., Kaihara, A., Sato, M., Tachihara, K. & Umezawa, Y. Split luciferase as an optical probe for detecting protein–protein interactions in mammalian cells based on protein splicing. *Anal. Chem.* **73**, 2516–2521 (2001).

34. Paulmurugant, R. & Gambhir, S. S. Monitoring protein–protein interactions using split synthetic *Renilla* luciferase protein-fragment-assisted complementation. *Anal. Chem.* **75**, 1584–1589 (2003).

35. Dixon, A. S. et al. NanoLuc complementation reporter optimized for accurate measurement of protein interactions in cells. *ACS Chem. Biol.* **11**, 400–408 (2016).

36. Kerppola, T. K. Design and implementation of bimolecular fluorescence complementation (BiFC) assays for the visualization of protein interactions in living cells. *Nat. Protoc.* **1**, 1278–1286 (2006).

37. Rebois, R. V. et al. Combining protein complementation assays with resonance energy transfer to detect multipartner protein complexes in living cells. *Methods* **45**, 214–218 (2008).

38. Héroux, M., Hogue, M., Lemieux, S. & Bouvier, M. Functional calcitonin gene-related peptide receptors are formed by the asymmetric assembly of a calcitonin receptor-like receptor homo-oligomer and a monomer of receptor activity-modifying protein-1. *J. Biol. Chem.* **282**, 31610–31620 (2007).

39. Armando, S. et al. The chemokine CXC4 and CC2 receptors form homo- and heterooligomers that can engage their signaling G-protein effectors and βarrestin. *FASEB J.* **28**, 4509–4523 (2014).

40. Fichter, K. M., Flajolet, M., Greengard, P. & Vu, T. Q. Kinetics of G-protein-coupled receptor endosomal trafficking pathways revealed by single quantum dots. *Proc. Natl. Acad. Sci. USA* **107**, 18658–18663 (2010).

41. Ahn, S., Shenoy, S. K., Wei, H. & Lefkowitz, R. J. Differential kinetic and spatial patterns of β-arrestin and G protein-mediated ERK activation by the angiotensin II receptor. *J. Biol. Chem.* **279**, 35518–35525 (2004).

42. Lohse, M. J., Maiellaro, I. & Calebiro, D. Kinetics and mechanism of G protein-coupled receptor activation. *Curr. Opin. Cell Biol.* **27**, 87–93 (2014).

43. Breton, B. et al. Multiplexing of multicolor bioluminescence resonance energy transfer. *Biophys. J.* **99**, 4037–4046 (2010).

44. Leduc, M. et al. Functional selectivity of natural and synthetic prostaglandin EP4 receptor ligands. *J. Pharmacol. Exp. Ther.* **331**, 297–307 (2009).

45. Rodriguez, E. A. et al. The growing and glowing toolbox of fluorescent and photoactive proteins. *Trends Biochem. Sci.* **42**, 111–129 (2017).

46. Inouye, S. & Shimomura, O. The use of *Renilla* luciferase, *Oplophorus* luciferase, and apoaequorin as bio-luminescent reporter protein in the presence of coelenterazine analogues as substrate. *Biochem. Biophys. Res. Commun.* **233**, 349–353 (1997).

47. Nagai, T. et al. A variant of yellow fluorescent protein with fast and efficient maturation for cell-biological applications. *Nat. Biotechnol.* **20**, 87–90 (2002).

48. Pfleger, K. D. G. & Eidne, K. A. Illuminating insights into protein-protein interactions using bioluminescence resonance energy transfer (BRET). *Nat. Methods* **3**, 165–174 (2006).

49. Molinari, P., Casella, I. & Costa, T. Functional complementation of high-efficiency resonance energy transfer: a new tool for the study of protein binding interactions in living cells. *Biochem. J.* **409**, 251–261 (2008).

50. Wampler, J. E., Hori, K., Lee, J. W. & Cormier, M. J. Structured bioluminescence. Two emitters during both the in vitro and the in vivo bioluminescence of the sea pansy, *Renilla*. *Biochemistry* **10**, 2903–2909 (1971).

51. Yamakawa, Y., Ueda, H., Kitayama, A. & Nagamune, T. Rapid homogeneous immunoassay of peptides based on bioluminescence resonance energy transfer from firefly luciferase. *J. Biosci. Bioeng.* **93**, 537–542 (2002).

52. Li, F. et al. Buffer enhanced bioluminescence resonance energy transfer sensor based on *Gaussia* luciferase for in vitro detection of protease. *Anal. Chim. Acta* **724**, 104–110 (2012).

53. Inouye, S., Sato, J., Sahara-Miura, Y., Yoshida, S. & Hosoya, T. Luminescence enhancement of the catalytic 19kDa protein (KAZ) of *Oplophorus* luciferase by three amino acid substitutions. *Biochem. Biophys. Res. Commun.* **445**, 157–162 (2014).

54. Inouye, S., Watanabe, K., Nakamura, H. & Shimomura, O. Secretional luciferase of the luminous shrimp *Oplophorus gracilirostris*: cDNA cloning of a novel imidazopyrazinone luciferase. *FEBS Lett.* **481**, 19–25 (2000).

55. Czupryna, J. & Tsourkas, A. Firefly luciferase and Rluc8 exhibit differential sensitivity to oxidative stress in apoptotic cells. *PLoS ONE* **6**, e20073 (2011).

56. Shigehisa, M. et al. Stabilization of luciferase from *Renilla reniformis* using random mutations. *Protein Eng. Des. Sel.* **30**, 7–13 (2017).

57. Hu, M.-J. et al. Development of a novel ligand binding assay for relaxin family peptide receptor 3 and 4 using NanoLuc complementation. *Amino Acids* **50**, 1111–1119 (2018).

58. Stoddart, L. A. et al. Development of novel fluorescent histamine H1-receptor antagonists to study ligand-binding kinetics in living cells. *Sci. Rep.* **8**, 1572 (2018).

59. Chu, J. et al. A bright cyan-excitable orange fluorescent protein facilitates dual-emission microscopy and enhances bioluminescence imaging in vivo. *Nat. Biotechnol.* **34**, 760–767 (2016).

60. Laviv, T. et al. Simultaneous dual-color fluorescence lifetime imaging with novel red-shifted fluorescent proteins. *Nat. Methods* **13**, 989–992 (2016).

61. Machleidt, T. et al. NanoBRET—a novel BRET platform for the analysis of protein–protein interactions. *ACS Chem. Biol.* **10**, 1797–1804 (2015).

62. Robbins, M. S. & Hadwen, B. J. The noise performance of electron multiplying charge-coupled devices. *IEEE Trans. Electron Devices* **50**, 1227–1232 (2003).

63. Basden, A. G., Haniff, C. A. & Mackay, C. D. Photon counting strategies with low-light-level CCDs. *Mon. Not. R. Astron. Soc.* **345**, 985–991 (2003).

64. Zacharias, D. A., Violin, J. D., Newton, A. C. & Tsien, R. Y. Partitioning of lipid-modified monomeric GFPs into membrane microdomains of live cells. *Science* **296**, 913–916 (2002).
65. Schink, K. O., Raiborg, C. & Stenmark, H. Phosphatidylinositol 3-phosphate, a lipid that regulates membrane dynamics, protein sorting and cell signalling. *Bioessays* **35**, 900–912 (2013).

Author contributions

M.B. and H.K. conceptualized the method, designed the experiments and wrote the manuscript. H.K. assembled the imaging system, performed the imaging experiments and analyzed the images. A.-M.S. and L.-P.P. designed and generated constructs for BRET microscopy. L.-P.P. performed the comparison between the spectrometric characteristics of the different luciferase constructs and participated in the writing of the manuscript.

Competing interests

The authors declare no competing interests.

Additional information

Supplementary information is available for this paper at https://doi.org/10.1038/s41596-019-0129-7.

Reprints and permissions information is available at www.nature.com/reprints.

Correspondence and requests for materials should be addressed to M.B.

Journal peer review information: *Nature Protocols* thanks Francisco Ciruela Alférez, Thomas Machleidt and other anonymous reviewer(s) for their contribution to the peer review of this work.

Publisher's note: Springer Nature remains neutral with regard to jurisdictional claims in published maps and institutional affiliations.

Related links
Key references using this protocol
Namkung, Y. et al. *Nat. Commun.* **7**, 12178 (2016): https://doi.org/10.1038/ncomms12178
Beautrait, A. et al. *Nat. Commun.* **8**, 15054 (2017): https://doi.org/10.1038/ncomms15054

naturereearch

Corresponding author(s):   Michel Bouvier

Reporting Summary

Nature Research wishes to improve the reproducibility of the work that we publish. This form provides structure for consistency and transparency in reporting. For further information on Nature Research policies, see <u>Authors & Referees</u> and the <u>Editorial Policy Checklist</u>.

Statistical parameters

When statistical analyses are reported, confirm that the following items are present in the relevant location (e.g. figure legend, table legend, main text, or Methods section).

n/a	Confirmed	
☐	☒	The <u>exact sample size</u> (*n*) for each experimental group/condition, given as a discrete number and unit of measurement
☐	☒	An indication of whether measurements were taken from distinct samples or whether the same sample was measured repeatedly
☐	☒	The statistical test(s) used AND whether they are one- or two-sided *Only common tests should be described solely by name; describe more complex techniques in the Methods section.*
☒	☐	A description of all covariates tested
☒	☐	A description of any assumptions or corrections, such as tests of normality and adjustment for multiple comparisons
☐	☒	A full description of the statistics including <u>central tendency</u> (e.g. means) or other basic estimates (e.g. regression coefficient) AND <u>variation</u> (e.g. standard deviation) or associated <u>estimates of uncertainty</u> (e.g. confidence intervals)
☒	☐	For null hypothesis testing, the test statistic (e.g. *F*, *t*, *r*) with confidence intervals, effect sizes, degrees of freedom and *P* value noted *Give P values as exact values whenever suitable.*
☒	☐	For Bayesian analysis, information on the choice of priors and Markov chain Monte Carlo settings
☒	☐	For hierarchical and complex designs, identification of the appropriate level for tests and full reporting of outcomes
☒	☐	Estimates of effect sizes (e.g. Cohen's *d*, Pearson's *r*), indicating how they were calculated
☐	☒	Clearly defined error bars *State explicitly what error bars represent (e.g. SD, SE, CI)*

Our web collection on <u>statistics for biologists</u> may be useful.

Software and code

Policy information about <u>availability of computer code</u>

Data collection	Metamorph 7.8.0. was used to collect the microscopy images
Data analysis	Metamorph 7.8.0 was used for BRET image processing, ratiometric calculation and image thresholding; Prism 7.03 for calculating basic statistical parameters and graph drawing; Microsoft Excel Office 365 for database; MATLAB 2016b for histogram analysis

For manuscripts utilizing custom algorithms or software that are central to the research but not yet described in published literature, software must be made available to editors/reviewers upon request. We strongly encourage code deposition in a community repository (e.g. GitHub). See the Nature Research <u>guidelines for submitting code & software</u> for further information.

Data

Policy information about <u>availability of data</u>

All manuscripts must include a <u>data availability statement</u>. This statement should provide the following information, where applicable:

- Accession codes, unique identifiers, or web links for publicly available datasets
- A list of figures that have associated raw data
- A description of any restrictions on data availability

The authors declare that all data supporting the findings in this study are presented within the article and are available from the corresponding author upon request.

nature research | reporting summary

April 2018

1

Field-specific reporting

Please select the best fit for your research. If you are not sure, read the appropriate sections before making your selection.

☒ Life sciences   ☐ Behavioural & social sciences   ☐ Ecological, evolutionary & environmental sciences

For a reference copy of the document with all sections, see nature.com/authors/policies/ReportingSummary-flat.pdf

Life sciences study design

All studies must disclose on these points even when the disclosure is negative.

Sample size	Data were repeated at least three (3) times
Data exclusions	No data were excluded from the analysis
Replication	All attempts at replication were successful
Randomization	No samples/organisms/participants were used in this study
Blinding	No samples/organisms/participants were used in this study, so no blinding was possible

Reporting for specific materials, systems and methods

Materials & experimental systems

n/a	Involved in the study
☒	☐ Unique biological materials
☒	☐ Antibodies
☐	☒ Eukaryotic cell lines
☒	☐ Palaeontology
☒	☐ Animals and other organisms
☒	☐ Human research participants

Methods

n/a	Involved in the study
☒	☐ ChIP-seq
☒	☐ Flow cytometry
☒	☐ MRI-based neuroimaging

Eukaryotic cell lines

Policy information about cell lines

Cell line source(s)	The HEK293 cell line used in this study is the one in which BRET-based biosensors have been developed in Dr Bouvier's laboratory.
Authentication	None of the cell line used were authenticated
Mycoplasma contamination	All cells were regularly tested for mycoplasma contamination (PCR Mycoplasma Detection kit, abm, BC, Canada)
Commonly misidentified lines (See ICLAC register)	No misidentified cell lines were used in this study